Polarization Effects Stabilize Bacteriorhodopsin's Chromophore Binding Pocket: A Molecular Dynamics Study

G. Babitzki, R. Denschlag, and P. Tavan*

Theoretische Biophysik, Lehrstuhl für Biomolekulare Optik, Ludwig-Maximilians-Universität, Oettingenstr. 67, 80538 München, Germany

Received: March 18, 2009; Revised Manuscript Received: May 25, 2009

Hybrid methods, which combine a quantum mechanical description of a chromophore by density functional theory (DFT) with a molecular mechanics (MM) model of the surrounding protein binding pocket, can enable highly accurate computations of the chromophore's *in situ* vibrational spectra. As a prerequisite, one needs a MM model of the chromophore−protein complex, which allows a correct sampling of its room-temperature equilibrium fluctuations by molecular dynamics (MD) simulation. Here, we show for the case of bacteriorhodopsin (BR) that MM−MD descriptions with standard nonpolarizable force fields entail a collapse of the chromophore binding pocket. As demonstrated by us, this collapse can be avoided by employing a polarized MM force field derived by DFT/MM hybrid computations. The corresponding MD simulations, which are complemented by a novel Hamiltonian replica exchange approach, then reveal a structural heterogeneity within the binding pocket of the retinal chromophore, which mainly pertains to the structure of the lysine chain covalently connecting the retinal chromophore with the protein backbone.

Introduction

The well-known membrane protein bacteriorhodopsin (BR) acts as a light-driven proton pump in the cell membrane of the archaebacterium *Halobacterium salinarum*. Since its detection by Oesterhelt and Stoeckenius,[1,2] an enormous amount of scientific effort has been devoted to uncover the physical mechanisms governing the structure and functional dynamics of this small molecular machine (for reviews see, e.g., refs 3 and 4). The popularity of BR in biophysics and beyond is due to its exceptional stability, its simple accessibility, and the rapid turnover of its light-triggered proton pump cycle: A few milliseconds after light absorption, the proton pumping is complete. The pumping proceeds through several intermediate states, whose optical and vibrational spectra are markedly different and show lifetimes ranging from pico- up to milliseconds. This spectroscopically detectable so-called photocycle is kinetically coupled to a vectorial proton transport across the membrane. The transport involves a series of de- and reprotonations of the chromophore and of various aspartic acids. As a consequence of BR's favorable properties, many spectroscopic methods have first been tested and established using BR as a sample system.

Particularly for the demonstration of how one can use the various variants of vibrational spectroscopy for a detailed characterization of dynamical processes in biomolecules, BR has been (and still is; see, e.g., refs 5−7) a testing ground.[8] Here, resonance Raman spectroscopy can shed light on structural transformations of the chromophore,[9−11] whereas infrared (IR) difference techniques additionally enable a detailed monitoring of light-induced changes within the surrounding protein matrix.[12] Both techniques can be applied at a very high (up to fs) time resolution to chromoproteins at ambient temperatures and therefore enable the observation of dynamical processes under quasi-native conditions.

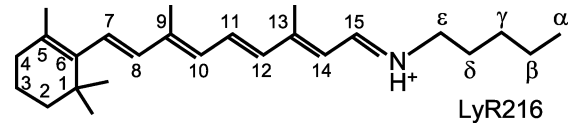

Figure 1. Chemical structure of the BR chromophore: In the light-adapted state BR_{568}, the chromophore is the protonated Schiff base of all-*trans* retinal ($RSBH^+$), which is covalently linked to the protein through Lys216, thus constituting a special residue called LyR216.

Unfortunately, it is generally not easy to decode the wealth of structural information contained in the vibrational spectra. Exceptions are, e.g., the spectrally well-separated bands of protonated carboxylic acids, whose involvement in proton transfer processes can therefore be observed in a kinetically resolved fashion.[13,14] In contrast, a particularly hard case is the BR chromophore when it comes to determine the structural meaning of the associated vibrational bands as they are observed in the course of the photocycle.[15−19] Nevertheless, for the light-adapted initial state BR_{568} of this cycle, the chromophore structure is quite precisely known[9] and is the protonated Schiff base of all-*trans* retinal depicted in Figure 1.

The positive charge, which is introduced into the retinal molecule by the protonation, delocalizes into the conjugated π-electron system and this mobile charge is the cause for the huge polarizability of an $RSBH^+$. Because of this polarizability, local electric fields generated by a condensed-phase environment (like, e.g., by a chromophore binding pocket of a protein) can steer the properties of an embedded $RSBH^+$ and, here, particularly the bonding properties within the π-conjugated chain. The optical and IR spectra of the chromophore are shaped by these properties. Because structural changes of the environment generally lead to changes of the local electric fields, such changes shift the spectral positions of prominent absorption bands in the optical and IR spectral regions.[19,20] The extraordinary sensitivity, with which an $RSBH^+$ changes its electronic structure in response to external fields, is the reason why this chromophore is an excellent spectroscopic probe for dynamical

* Corresponding author. E-mail: tavan@physik.uni-muenchen.de. Phone: +49-89-2180-9220. Fax: +49-89-2180-9202.

10.1021/jp902428x CCC: $40.75
Published on Web 07/06/2009

processes in a protein. On the other hand, this sensitivity is also the main cause for the challenge, which this chromophore poses to theoretical descriptions.

Computational Approaches to the Chromophore's IR Spectra. About 15 years ago, density functional theory[21,22] (DFT) was converted into an easily accessible tool for computing the ground-state properties of isolated molecules.[23] Since then, accurate computations of gas-phase vibrational spectra have become standard software applications.[24−26] However, for molecules embedded in polar solvents or in proteins, the strong electrostatic interactions with the environment have to be included in the DFT Hamiltonian.[27] Because the electrostatic interactions are long-ranged and because the polarizability of an $RSBH^+$ is very large, the condensed-phase environments capable of polarizing such a chromophore comprise too many atoms to be included in a DFT treatment at a manageable computational cost. Therefore, one has to resort to simplified molecular mechanics (MM) models that can approximately account for the electrostatics of the chromophore's environment.

A corresponding DFT/MM hybrid method was designed by Eichinger et al.[28] to enable accurate computations of a chromophore's vibrational spectra in a condensed-phase environment. Subsequent applications of this method to quinones in the reaction center of *Rb. sphaeroides* and in aqueous solution,[29,30] as well as to various molecules in solution,[31−36] demonstrated the merits and remaining deficiencies of this hybrid method. Like all other hybrid methods, which describe a small fragment of a simulation system by a quantum mechanical (QM) Hamiltonian and the remainder by an MM force field (see ref 28 for extended references), also the quoted DFT/MM approach conceptually derives from the seminal work of Warshel and Levitt.[37] Its key merit is a careful treatment of covalent bonds linking the QM and MM fragments which removes corresponding artifacts from the vibrational spectra of the QM fragment, hampering previous methods (see ref 28 for details).

As discussed in a recent review,[27] the mid-IR spectra of molecules in a condensed-phase environment can be calculated by DFT/MM at a comparable accuracy as the gas-phase spectra by DFT, as long as these molecules are at most mildly polar. In contrast, charged solute molecules like, e.g., phosphate ions[31,38] will strongly polarize their solvent environment and will thus be exposed to a strong reaction field that can cause very large shifts of the solute's vibrational bands. In conventional MM force fields, however, the dynamic electronic polarizability is neglected. Thus, for charged solute molecules, such force fields underestimate the strength of the reaction field and the associated solvatochromic shifts of the vibrational bands.[27]

Using meanwhile established computational protocols,[33] one can accurately calculate by DFT/MM not only the frequencies but also the inhomogeneously broadened shapes and intensities of the mid-IR bands of a solute molecule. Among these protocols, the so-called "instantaneous normal-mode analysis" (INMA) is computationally the least demanding. Here, one employs a standard MM molecular dynamics (MD) simulation to generate a set of solvent−solute structures, which should be representative of the equilibrium fluctuations at room temperature. Subsequently, the solvent cages of these MM−MD snapshots are kept fixed and a series of vibrational line spectra is calculated for the solute by means of DFT/MM normal-mode analysis. Other protocols, in contrast, need a very costly DFT/MM−MD simulation that has to cover at least several tens of picoseconds (see ref 33 for a comparative discussion). Thus, the condensed-phase vibrational spectra of large molecules (like a peptide in solution[34] or the $RSBH^+$ in BR) can be currently computed only through the INMA protocol in an accurate and computationally manageable fashion.

One may ask why accurate computations of the vibrational spectra of the BR chromophore in the various states of the pump cycle are still of interest (and even required, if one wants to gain a physical understanding of the pump mechanism in BR). This question will be addressed in part II of this work (DOI 10.1021/jp902432e), which presents our DFT/MM results on the IR spectra of the BR chromophore obtained by the INMA approach. Instead, here, we address the question as to how one can obtain by MM−MD simulations a set of structural snapshots for the $RSBH^+$ in the BR binding pocket, which correctly represents the room-temperature equilibrium ensemble and, thus, provides a valid starting point for part II (DOI 10.1021/jp902432e). In fact, this task turned out to be technically much harder than the subsequent DFT/MM computation of the IR spectra from a given snapshot ensemble.

This paper is organized as follows: First, we review previous MM−MD descriptions of BR_{568} which, by applying standard force fields, tried to model the equilibrium conformational fluctuations. We show that these descriptions fall short of explaining the corresponding experimental evidence. By arguing that this failure is due to the neglect of the electronic polarizability in standard MM force fields, we offer our working hypothesis. Extended MD simulations of BR, which compare standard force fields with polarized force fields derived from DFT/MM calculations, subsequently serve us to provide evidence for the validity of our hypothesis. Here, we first describe in some detail the computational methods employed in the simulations, in the DFT/MM computations of polarized force fields, and in the statistical data analysis. Next, we present the results and particularly discuss the issue of structural heterogeneity emerging from the simulation data. A short summary and outlook concludes the paper.

BR_{568}—A Challenge for MM−MD

Already in 1999, the complexities of the task to generate by MM−MD a set of snapshot structures, which correctly represents the room-temperature structural ensemble within the chromophore binding pocket of BR_{568}, started to show up in the thesis of Eichinger.[39] This thesis reports first attempts to describe the IR spectra of the BR chromophore by a DFT/MM approach. At that time, the high-resolution X-ray structure 1C3W of BR was still unknown.[40] According to this structure and as shown in Figure 2, in BR, the chromophore binding motif is composed of four key charged residues, which form a neutral but strongly quadrupolar charge distribution. This charge distribution is located near the center of the membrane. As follows from dynamics modelings (see, e.g., further below), the charge distribution is stabilized by a hydrogen bonded network. This network is generated by three water molecules, which are also shown in Figure 2 with their oxygen atoms at the crystallographic locations.

Instead of this high-resolution structure, Eichinger[39] had to choose lower resolution models like those of Grigorieff et al.[41] or Essen et al.[42] as starting points for the computation of IR spectra. Because these models contained no water molecules at all, such molecules had to be added by cavity filling. In this process, a water molecule was always initially modeled into the position of the water molecule W_1 in Figure 2,[39] because room-temperature spectroscopic evidence had clearly indicated that the Schiff base proton must be stably hydrogen bonded to a water molecule. This hydrogen bonding motif had been first

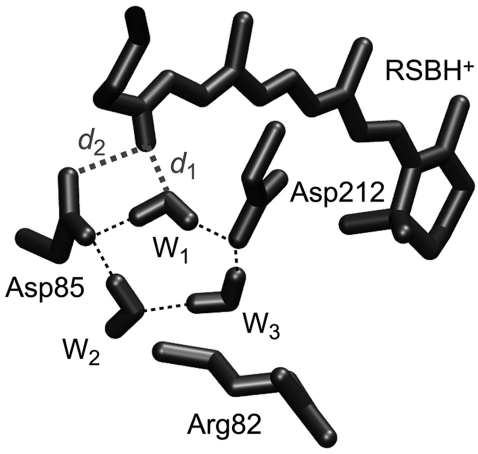

Figure 2. Hydrogen bonded network (black dashed lines) linking the key charged residues and the three water molecules in the chromophore binding pocket of BR. This network follows from the high-resolution (1.55 Å) crystal structure 1C3W[40] by applying the modeling and simulation procedures described in Methods. The distances (gray dashed lines) between the Schiff base proton and the oxygen atom of the closest water molecule (d_1) or the closest oxygen of Asp85 (d_2), respectively, can serve as measures for the stability of the depicted structure.

detected by Hildebrandt and Stockburger[43] using a clever argument on the changing line width of the C=N stretching band observed in the resonance Raman spectrum of BR_{568} upon H_2O/D_2O exchange. The subsequent confirmation[44] by high-resolution, solid-state ^{15}N NMR has additionally shown that the hydrogen bond between the Schiff base proton and a water molecule stably persists on the extended time scale of such measurements.

In the study of Eichinger,[39] the apoprotein was modeled by the standard CHARMM22 force field[45] and the chromophore as well as part of the lysine chain (cf. Figure 1) by DFT. Encouragingly, the IR line spectra of the chromophore calculated by DFT/MM for the quoted structural models were much closer to the well-known experimental data[46,47] than IR spectra calculated by DFT for an isolated $RSBH^+$. Nevertheless, the calculated spectra also showed marked differences (i) from each other and (ii) from the experimental spectra, indicating (i) that small differences among the chosen molecular models are magnified by the polarizability of the $RSBH^+$ into sizable spectral line shifts and (ii) that the chosen models are most probably not quite correct.

Is BR's Chromophore Binding Pocket Stable in MM−MD? Line spectra derived by DFT/MM from a static model of a low-temperature protein structure are not the kind of theoretical predictions that one should compare to room-temperature vibrational spectra. Instead, one should try to get access to the room-temperature ensemble of chromoprotein configurations to additionally model the fluctuations of the vibrational lines and, thus, to get access to the band shapes. However, when Eichinger[39] tried to generate such an ensemble by MM−MD simulations for water soaked BR models,[41,42] he observed that these structures "collapsed". Thus, an INMA computation of the IR spectra was not feasible and either the employed MM force field (CHARMM22), the positions of the added water molecules, the experimental starting structures, or all of that seemed to be too inaccurate for generating stable equilibrium ensembles of BR by MM−MD.

Meanwhile, the 1.55 Å structure of Luecke et al.[40] has removed the uncertainties concerning the experimental low-temperature structure of BR_{568}. Furthermore, the NMR analysis of BR carried out by Patzelt et al.[48] has shown that the structural arrangement of the four charged groups and three water molecules depicted in Figure 2 is stably maintained also at room temperature. Finally, the recent FTIR study of Garczarek and Gerwert[5] has clearly confirmed that in BR_{568} this structural arrangement remains rock-solid at room temperature.

Interestingly, huge unconstrained MM−MD simulations of BR trimers embedded in a periodic membrane/water solvent model showed a different picture.[49−51] For instance, Kandt et al.[50] stated for "the triple water cluster... near the Schiff base" (and depicted in Figure 2) that the "MD simulation shows highly mobile waters with fluctuations of 4 Å per individual water molecule". Furthermore, the pictures, which are given in the quoted paper as illustrations for the resulting "water density" (Figure 4a and b in ref 50), clearly indicate that the Schiff base proton was hydrogen bonded to Asp85 in this simulation. Thus, the hydrogen bond of the Schiff base group with a water molecule, which stably persists in BR on the time scale of NMR measurements, actually decayed within the 5 ns of the quoted MD simulation. Grudinin et al.[51] using a similarly extended simulation model likewise found that the water molecule denoted as W_1 in Figure 2 left its crystallographic position. Also, the MM−MD simulations of Eichinger[39] consistently showed a decay of the initially modeled hydrogen bond between the Schiff base proton and the water molecule W_1 followed by the formation of a new hydrogen bond between the Schiff base proton and Asp85. Eichinger[39] considered this conformational transition as a structural "collapse" and concluded that his MM−MD simulations cannot provide any insight into the equilibrium structure and fluctuations of the BR binding pocket. Kandt et al.[50] and Grudinin et al.,[51] while stating the difference of their MM−MD simulations with the X-ray data, attributed this difference solely to the simplicity of the employed water model and were apparently quite content with the fact that W_1 stayed at least near its crystallographic position during their 5 and 2.5 ns simulations, respectively.

Concerning the MM−MD methodology, it is important to note that Kandt et al.[50] employed the GROMACS[52,53] force field for the apoprotein and the associated simple point charge (SPC) model for the water molecules, that Grudinin et al.[51] used AMBER for the protein and the three-point transferable interaction potential[54] [TIP3P] for the water molecules, and that Eichinger[39] used CHARMM22 combined with TIP3P.[45] Despite these force field differences, the same type of structural decay occurred in all three studies.

That this type of structural decay seems to be a general feature of conventional nonpolarizable MM force fields can be concluded from the MD study of Hayashi et al.[55] who noted "that the TIP3P/AMBER force field, in which nonbonding interactions are described by only classical pairwise potential functions, cannot even reproduce the conformation of Wat402 observed in the X-ray ground-state structure; after the MD equilibration, the Schiff base N−H bond directly attaches to O_2 of Asp85." With GROMACS, CHARMM22, and AMBER, the three most widespread conventional MM force fields for proteins thus showed the same failure in MD simulations of BR: The water molecule, which according to the available experimental evidence is stably attached to the Schiff base proton, apparently does not want to stay at this position. Instead, the $RSBH^+$ and Asp85 are predicted to form a stable ion pair. We will denote the resulting non-native conformation by C_{nn}.

Therefore, one expects that this structural decay into conformation C_{nn} will also occur in MM−MD simulations with the TIP3P/CHARMM22 force field, in which a BR model

deriving from the high-resolution structure 1C3W is employed.[40] As we will show further below, this is actually the case.

Possible Sources of the Apparent Force Field Deficiencies. Hayashi et al.[55] fixed the problem of structural decay by introducing additional local potential functions capable of constraining the water molecule W_1 at the experimental position. Furthermore, they used instead of the static TIP3P water model the polarizable potential function of Rick et al.[56] These choices for fixing the apparent force field bugs were motivated by a certain interpretation of QM/MM results,[57] which attributed the considerable stability of the hydrogen bond between the $RSBH^+$ and the water molecule W_1 mainly to local charge transfer effects. However, because the quoted QM/MM study[57] did not compare the native arrangement shown in Figure 2 with the ion pair structure ($RSBH^+\cdots Asp85^-$), it cannot answer the question of why the conventional MM force fields erroneously prefer the ion pair over the experimentally observed hydrogen bonded network. Therefore, it is uncertain whether this MM−MD failure is caused by an inaccurate modeling of certain local effects (refs 55 and 57) or is due to more general properties of conventional MM force fields.

Because we generally hold the view that the main shortcoming of conventional MM force fields is their systematic neglect of the dynamic electronic polarizability,[58,59] in this paper, we will address the question as to whether the inclusion of polarization effects into the protein force field can stabilize the chromophore binding pocket of BR at the experimental structure in extended MM−MD simulations. In the given case, such a stabilization by polarization seems likely, because the key structural motif consists of four charged residues in the low-dielectric center of a membrane, where the associated Coulomb fields are poorly screened and, thus, are strong sources of electronic polarization.

To keep the focus on the polarization of the protein, we will maintain the nonpolarizable TIP3P model for the water molecules in our extended MD simulations. We will, however, check by DFT/MM calculations to what extent the electronic polarizability of the three water molecules in the chromophore binding pocket can contribute to the stabilization of the experimental structure. Note in this context that conventional water models like TIP3P include a mean field description of polarization effects through the assumption of a "condensed-phase" dipole moment that is much larger than the dipole moment of an isolated water molecule (see ref 35 for a recent discussion of water polarizability). Whether this mean polarization applying to bulk water suffices for the three water molecules in the hydrophobic center of BR is to be seen.

Methods

Setup of a Simulation Model for BR. For the construction of a BR simulation model, we chose the 1.55 Å X-ray structure 1C3W as our starting point.[40] Trial coordinates for the hydrogen atoms and for residues, which are missing in the 1C3W data set (Thr157-Glu161, Glu232, Ala233), were added with the help of the MD program X-PLOR.[60] Next, the CHARMM22 force field[45] was assigned to the protein, the TIP3P model[54] to the crystallographic water molecules, and an MM model to the $RSBH^+$ (see further below).

With the exception of the four charged residues in the center of the membrane (see Figure 2) and of two glutamates, which are located in the extracellular proton release channel relatively close to the $RSBH^+$, all other titratable groups were chosen as neutral. There are several titratable groups (including the C- and N-termini) near the two water-exposed surfaces of BR, which should be charged at a pH of 7. The neutralization of these groups serves as a crude model for the strong dielectric shielding of their Coulomb potentials by the aqueous environment. Near the center of the membrane, there is no such shielding and, therefore, in this region the charges of titratable groups were chosen as given by experimental evidence.[61−63] Correspondingly, a negative charge was assigned to Asp85 and Asp212, a positive charge to Arg82 and LyR216, and no net charge to Asp96 and Asp115. To account (i) for the presence of a delocalized proton in the extracellular proton release channel of BR[5,64] and (ii) for the partial dielectric shielding in the associated region at the boundary between the hydrophobic core of the membrane and the water-exposed extracellular surface, a charge of $-0.5\ e$ was assigned to each of the two glutamates (Glu194 and Glu204), marking the exit of the proton release channel.

In a series of annealing MD simulations, in which all crystallographically determined coordinates of heavy atoms were kept fixed, the hydrogen and the other modeled atoms were allowed to adjust to the X-ray structure. As a result, for instance, the hydrogen bonded network shown in Figure 2 became apparent and the water molecules assumed the depicted orientations.

Because the charge distribution of BR polarizes the high-dielectric aqueous phases on the two sides of the purple membrane, the induced orientational polarization generates a reaction field acting back on the BR charge distribution. To provide a simple model for this reaction field, we attached two water caps comprising a total of 246 additional water molecules to the two water-exposed surfaces of BR. The caps were allowed to diffuse into the surfaces in a multiple stage computational relaxation process:

In a sequence of 300 K MD simulations, most protein atoms were allowed to move freely. Solely the positions x of the C_α atoms and of the heavy atoms of the special residue LyR216 were constrained by harmonic potentials $k_c(\mathbf{x} - \mathbf{x}_c)^2$ with the stiff force constants $k_c = 6$ kcal/(mol·Å^2) to the crystallographic positions $\mathbf{x}_c$. These stiff constraints restrict thermal fluctuations to a root-mean-square deviation (rmsd) of about 0.3 Å and, thus, exclude large deviations from the X-ray structure at the backbone and at the chromophore. Furthermore, the added water molecules were constrained by soft harmonic potentials [k_c = 0.5 kcal/(mol·Å^2)], allowing fluctuations with an rmsd of about 1.1 Å to certain initial positions. These positions were given by the average positions in the respective preceding simulation (in contrast, the crystallographic water molecules were always bound by soft potentials to their X-ray positions). For the added water molecules, the resulting stationary positions served in all following MM−MD simulations as centers of constraining soft potentials. Here, most crystallographic water molecules remained softly constrained to the experimental positions. An exception were the members W_1-W_3 of the central water cluster, which were left unconstrained. The thus obtained structural model of BR preserves the key features of the original X-ray structure and, therefore, is called 1C3W/MD.

For the sake of computational efficiency, the MD simulation model 1C3W/MD contains as few atoms as possible and nevertheless, for the sake of accuracy, covers key aspects of the complicated and inhomogeneous dielectric environment represented by a membrane/water system. It is well-known that a model of a membrane protein, which omits the membrane and most of the surrounding water for reasons of computational efficiency, can be stable in extended MD simulations only if at least part of the system is constrained at the experimental

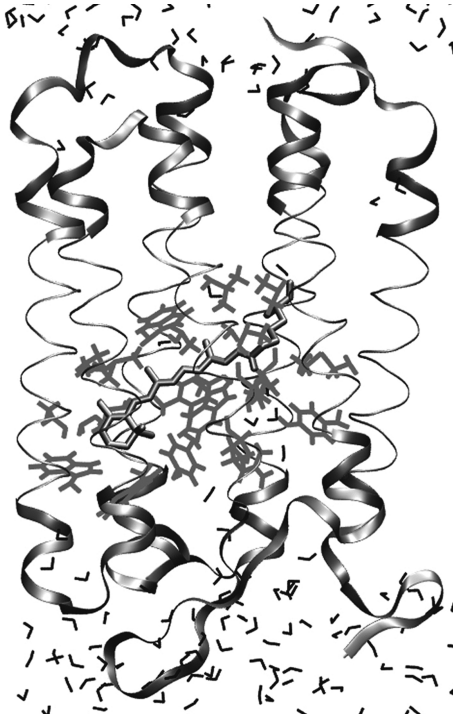

Figure 3. BR model for partially constrained MD simulations and for the computation of a polarized force field. The backbone of residues, whose C_α atoms are constrained by stiff harmonic potentials to the crystallographic positions,[40] is drawn as a wide loop; the backbone of unconstrained residues is indicated by a thin circular drawing style. Water molecules are represented as small black hooks. The residues, whose partial charges are calculated by DFT/MM to generate a polarized force field, are drawn as light-gray structural models.

positions.[65] Because we are solely interested in the thermal fluctuations of all those BR atoms, which are located near the chromophore within the core of the membrane, we constrained the C_α atoms of residues near the extra- and intracellular surfaces by stiff harmonic potentials to the crystallographic positions.

As shown in Figure 3, the unconstrained part of the simulation system forms a slab in the center of and oriented parallel to the membrane. The slab covers at least four windings of each of the seven transmembrane helices. Thus, its thickness along the membrane normal is everywhere larger than 22 Å. In its center, the slab contains the chromophore, whose extension along the membrane normal is about 8 Å.

The specification of the simulation setup is complete as soon as also a MM force field for the BR chromophore is given, because protein force fields like CHARMM22 solely cover parameters for standard molecular components of proteins. Thus, the parameters of the Lennard-Jones potentials for the various atom types in $RSBH^+$ were adopted from CHARMM22 parameters of atom types occurring in similar structural motifs. By the same analogy modeling, also the force constants of the harmonic bond stretch and angle deformation potentials were chosen.[39] In contrast, the equilibrium values of the bond lengths and angles entering these potentials were taken as averages from a series of DFT/MM calculations of the $RSBH^+$ embedded in the BR binding pocket. Also, the partial charge distribution within the $RSBH^+$ was extracted from these calculations. The details of these calculations are given further below. The parameters of the torsional potentials for the dihedral angles within the polyene chain were estimated from the quantum chemical results on $RSBH^+$ model chromophores and the accompanying analysis of experimental data in ref 66. These parameters are listed in Table 1. For the remaining torsional

TABLE 1: Heights ΔE of Torsional Potentials in BR's $RSBH^+$[a]

double bonds		single bonds	
bond	$\Delta E^{\%}$	bond	$\Delta E^{\%}$
C5═C6	32	C6—C7	5
C7═C8	28	C8—C9	8
C9═C10	26	C10—C11	12
C11═C12	23	C12—C13	16
C13═C14	20	C14—C15	20
C15═N	30		

[a] % energies are given in kcal/mol.

potentials, which are required to define MM models for the cyclohexene ring, for the methyl groups attached to the polyene chain, and for the lysine chain, parameters were chosen which in CHARMM22 are standard for such structural motifs.[39]

Among all of these force field parameters, there are only a few which are of key importance for MM—MD simulations and all of them pertain to the conjugated chain within BR's $RSBH^+$. These parameters are the partial charges, which sensitively depend on the electric field within the binding pocket and steer the important electrostatic interactions with the surroundings, the torsional potentials, which steer the possible deviations of the $RSBH^+$ from planarity, and the equilibrium values of the bond angles, which steer the banana-shaped curvature of the $RSBH^+$ (for the importance of the torsional potentials, see refs 66—68). As explained above, these key parameters were either derived from *in situ* DFT/MM descriptions or from a previous quantum chemical analysis.[66]

MM—MD Simulation Procedures. The MM—MD simulations were carried out with the program package EGO/MMII,[69] which combines a hierarchy of fast structure-adapted multipole expansions for the efficient treatment of the long-range electrostatics[70,71] with a multiple time-step integrator.[72,73] A period of 1 fs was chosen as the basic time step of this integrator. The bond lengths of the hydrogen atoms were kept constant using the M-SHAKE algorithm[74] with a relative tolerance of 10^{-6}. The temperature of the system was kept at 300 K by coupling one Berendsen thermostat[75] to the protein atoms and another one to the water molecules (with the exception of the three water molecules near the $RSBH^+$). As time constants of thermostat couplings, we chose 0.5 ps. Two separate thermostats were applied to the protein and the water subsystems to avoid the so-called "hot-solvent/cold-solute" problem.[76]

Using different force fields for the apoprotein, we carried out several MD simulations at 300 K with durations in the range 10—50 ns. In all of these simulations, the general starting model 1C3W/MD, in which all C_α atoms are still stiffly constrained to the crystallographic positions, was converted into the partially unconstrained simulation model sketched in Figure 3 by a 150 ps equilibration simulation during which the constraints at the C_α atoms in the central slab were removed and the system was tempered to 300 K. A second 1 ns equilibration phase preceded the trajectories used for data acquisition.

The force fields employed in these MD simulations differed in the partial charges assigned to the 23 residues forming the binding pocket of the $RSBH^+$. We either chose the standard CHARMM22 partial charges[45] or partial charges obtained by iteratively applying the DFT/MM hybrid method of Eichinger et al.[28] to certain BR structures. The resulting sets of partial charges then define various structure-adapted polarized force fields. Following ref 77, one could call the approach applied by us to the computation of an improved electrostatic potential within BR also a partial "moving domain" DFT/MM method,

which is partial because it has been solely applied to the central region of BR containing the chromophore and its neighborhood (for a general discussion, we refer to ref 77).

Calculation of Polarized Force Fields. One of the BR structures chosen for the computation of a polarized force field (called PBR) was our general starting model 1C3W/MD. For the DFT/MM hybrid computation of partial charges, all 23 residues were chosen, which in 1C3W/MD have at least one atom at a distance smaller than 4 Å from the $RSBH^+$. Each DFT/MM computation requires a partition of the whole structure 1C3W/MD into a DFT and a MM fragment. The partition is defined by specifying those C−C single bonds, at which the covalent linkage between the two fragments is cut using the "scaled position link atom method" (SPLAM).[28]

By cutting for most of the selected residues (Met20, Val49, Ala53, Tyr57, Tyr83, Trp86, Thr89, Thr90, Leu93, Met118, Trp138, Ser141, Thr142, Met145, Trp182, Tyr185, Pro186, Trp189, and Ala215) the $C_\alpha-C_\beta$ bond, the DFT treatment was restricted to the respective side chain. For the four charged residues Asp85, Asp212, Arg82, and LyR216 in the center of BR, however, also a piece of the backbone was included. Here, for the respective residue i, two SPLAM cuts were applied to the $C_{\alpha,i-1}-C'_{i-1}$ and $C_{\alpha,i}-C'_i$ bonds.

The DFT calculations were carried out with the plane-wave code CPMD[78] using the gradient-corrected exchange functional of Becke,[79] the correlation functional of Perdew,[80] and the norm-conserving pseudopotentials of Troullier and Martins.[81] The rectangular box containing the grid for the plane-wave expansion of the Kohn−Sham orbitals was placed around the respective DFT fragment in such a way that no atom of the fragment came closer than 3 Å to one of the faces and that the box volume became minimal. The size of the basis set was then defined by a cutoff of 70 Ry. The electrostatic potential generated by the MM fragment was imported into the respective DFT Hamiltonian as described in ref 28. So-called "ESP" partial charges were calculated for the DFT fragment by optimizing the match with the electrostatic potential, which is due to the enclosed charge distribution, at the van der Waals surface of the fragment.[82] After each DFT/MM calculation on one of the residues, its previous partial charges were replaced by these new ESP charges. This procedure, which started at the CHARMM22 partial charges, was iterated several times over the whole list of selected residues until the ESP charge distribution became stationary. Note that in each cycle the DFT/MM calculations started at LyR216 up to the last cycle which also ended with LyR216.

The thus obtained ESP charges, which characterize the polarized force field PBR, are listed for the 23 residues in Tables 2−9 provided online as Supporting Information (SI). In addition to our X-ray-based starting model 1C3W/MD, we applied this DFT/MM approach for computing a polarized force field to several further structural models, which were obtained as snapshots from MD simulations (see the Results and Discussion).

Generation of Free Energy Maps. As indicators, to what extent the chromophore binding pocket maintains its structure during the MD simulations, we used the two conformational coordinates d_i, $i = 1, 2$, defined in Figure 2 and in the associated caption. For the computation of the d_i, we extracted from each MD trajectory every 500 fs the distances $\delta_\alpha(t)$ between all of those oxygen atoms α and the Schiff base proton, which are possible hydrogen bonding partners of the $RSBH^+$. The atoms α comprise the oxygens of the three water molecules ($\alpha = 1, 2, 3$) in the binding pocket and the two oxygens ($\alpha = 4, 5$) of Asp85. The trajectories $\delta_\alpha(t)$ obtained in the various simulations are documented either in the Results and Discussion or in the SI. By the nearest neighbor criterion explained in the caption to Figure 2, the trajectories $\delta_\alpha(t)$ with $\alpha = 1, 2, 3$ were reduced to a data set $d_1(t)$ and those with $\alpha = 4, 5$ to a set $d_2(t)$.

The data sets $d_i(t)$ were converted into free energy landscapes $\Delta G(d_1,d_2)$. For this purpose, the rectangle [1.25 Å, 4.5 Å] × [1.25 Å, 4.25 Å] within the (d_1,d_2)-plane was subdivided into 31 × 33 bins and histogram density estimates $p(d_1,d_2)$ were evaluated from the distance data sets. The free energy then is $\Delta G(d_1,d_2) = -k_B T \ln p(d_1,d_2) - G_0$, where k_B is the Boltzmann constant and G_0 is a constant serving to set the minimum of ΔG to zero. Because empty bins in the histogram density estimate [$p(d_1,d_2) = 0$] would lead to infinite free energies, an upper energy cutoff $\Delta G_{max} = -k_B T \ln(1/M_{max})$ was introduced, where M_{max} is the maximum bin count found in the histogram, and ΔG was set to ΔG_{max} at all empty bins. A nearest neighbor smoothing was applied before generating the contour plots of $\Delta G(d_1,d_2)$.

Conformational Analysis of the Lysine Chain. To explore the equilibrium conformational ensemble of the aliphatic chain connecting in LyR216 the $RSBH^+$ with the backbone, we have used a Hamiltonian replica exchange (HRE) approach.[83−85] Like in conventional temperature replica exchange,[86,87] the Metropolis criterion

$$P_{ij} = \min[1, \exp(-\Delta_{ij})] \tag{1}$$

controls the exchange of two replicas i and j at neighboring temperatures $T_i < T_j$. In HRE, however, the difference Δ_{ij} has to account additionally for different Hamiltonians $H_i(X)$ and $H_j(X)$ of the replicas at the temperatures T_i and T_j:

$$\Delta_{ij} = \beta_i[H_i(X_j) - H_i(X_i)] + \beta_j[H_j(X_i) - H_j(X_j)] \tag{2}$$

Here, X_i and X_j denote the configurations of the replicas before exchange, β is $(1/k_B T)$, and k_B is the Boltzmann constant.

Our HRE approach closely resembles the replica exchange with solute tempering (REST) method introduced by Liu et al.[85] The differences pertain to the partitioning of the simulation system. Whereas in REST a peptide is heated and the surrounding solvent remains "cool" through scaling of the Hamiltonian, in our HRE, the lysine chain from C_β to C_ϵ is heated and the remainder of the simulation system stays "cool" upon scaling.

For a more specific explanation, we denote the lysine−lysine, lysine−remainder, and remainder−remainder interactions by L, LR, and R distinguishing additionally some of the bonded (b) and nonbonded (nb) interactions. We choose for a temperature T and the sampling temperature T_0 the Hamiltonian H by

$$H = H_L + H^b_{LR} + \sqrt{\frac{T}{T_0}} H^{nb}_{LR} + \frac{T}{T_0} H_R \tag{3}$$

This choice reduces eq 2 to

$$\Delta_{ij} = (\beta_j - \beta_i)\{[H_L(X_i) + H^b_{LR}(X_i)] - [H_L(X_j) + H^b_{LR}(X_j)]\} + (\sqrt{\beta_j\beta_0} - \sqrt{\beta_i\beta_0})[H^{nb}_{LR}(X_i) - H^{nb}_{LR}(X_j)] \tag{4}$$

This expression shows that the difference Δ_{ij} entering the exchange probability (1) is calculated from the potential energy of the lysine chain (including its interactions with the remainder), because the much larger term H_R cancels. The small number N

of degrees of freedom in the lysine chain leads to smaller shifts of the potential energies at neighboring temperatures such that the exchange criterion is frequently met even for large temperature distances. As a result, HRE allows us to cover the temperature range from 300 up to 660 K with only five replicas ($T_i \in \{300, 360, 440, 540, 660\ \mathrm{K}\}$) and an average exchange probability P_{ij} between neighboring replicas ($j = i \pm 1$) of about 40%. The HRE sampling was extended to 30 ns, and exchanges were attempted every 5 ps.

To identify the conformations of the lysine chain, we applied the hierarchical clustering approach described by Carstens et al.[88] in a paragraph entitled "Determination of the Conformational Ensembles". In short, we extracted from the HRE trajectory at the target temperature $T_0 = 300$ K every 5 ps the five torsional angles $\psi_k(t)$, $k = 1, ..., 5$, which belong to the five single bonds connecting the Lys216 C_α atom with the N atom of the $RSBH^+$ (cf. Figure 1). The resulting data set $\mathcal{X}$ covered 6000 five-dimensional vectors $\Psi(t)$ in the cyclic space $[0, 2\pi]^5$. Using a mixture of 100 five-dimensional, univariate, and cyclic normal distributions with equal weights and widths, a maximum likelihood estimate $\rho(\Psi)$ was calculated for the data density in $\mathcal{X}$ by applying the algorithms suggested in refs 89 and 90. Convolution of $\rho(\Psi)$ with Gaussians of varying widths yielded a scale space of successively smoothed model densities $\rho(\Psi|\sigma)$, whose maxima indicate for each resolution scale σ the prototypical conformations. The SI documents the details of this hierarchical conformational analysis, which safely identifies the minima of free energy landscapes in high-dimensional spaces at varying resolutions.

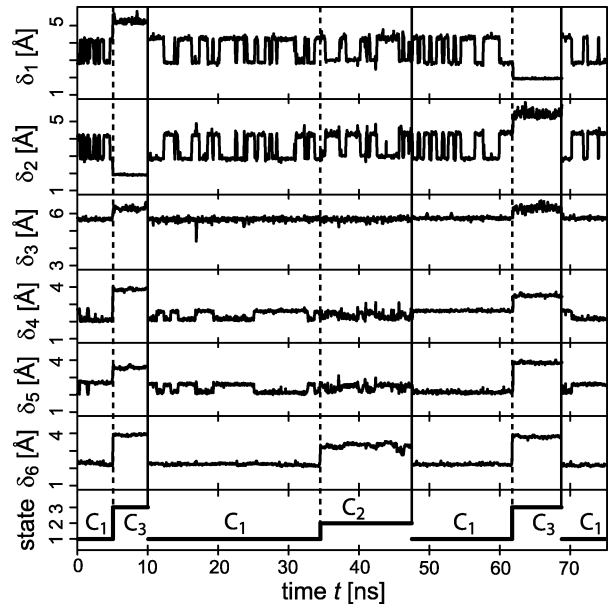

Figure 4. Trajectories of six distances $\delta_\alpha(t)$, $\alpha = 1, ..., 6$, and of a classification of the lysine chain into three conformational states C_1, C_2, and C_3 obtained from four CHARMM22-MD simulations at 300 K each starting at the structure 1C3W/MD (total duration: 75 ns). The first five δ_α measure the distances between the Schiff base proton and the five oxygen atoms, which are possible hydrogen bonding partners ($\delta_1-\delta_3$ for the water molecules W_1-W_3 and δ_4 and δ_5 for Asp85). δ_6 is the distance between the backbone carbonyl oxygen of LyR216 and the amide hydrogen of Gly220. For a discussion, see the text.

Results and Discussion

Here, we first demonstrate that our partially constrained MD simulation model for BR (cf. Figure 3) exhibits, for a conventional nonpolarizable force field, the same type of structural instability and decay into the non-native conformation C_{nn}, which was previously observed with such force fields by Kandt et al.[50] for an unconstrained protein trimer in a huge membrane/water system and by Eichinger[39] and Hayashi et al.[55] for partially constrained monomeric models.

CHARMM Instability of 1C3W/MD. To analyze the equilibrium fluctuations, which are predicted by the CHARMM22 force field for our BR model, we have carried out four MD simulations at 300 K covering a total of 75 ns as described in Methods. Figure 4 depicts the resulting trajectories for six selected distances δ_α, $\alpha = 1, ..., 6$, capable of indicating the stability of the chromophore binding pocket. In the bottom panel, the figure additionally displays the trajectory of a classification, which assigns to each sampled configuration of the aliphatic chain connecting the $RSBH^+$ with the protein backbone one of three conformational states C_k (this classification will be explained further below). The trajectories were sampled every 500 fs. The resulting data sets were smoothed and reduced by combining 100 consecutive data points into 50 ps averages.

Each of the four CHARMM22 simulations started at the initial structure 1C3W/MD (in Figure 4, these simulations are separated by vertical solid lines). In each simulation, the protein was found (bottom panel) to relax immediately into a first conformational state. Here, LyR216 maintains its initial structure, which is characterized by the conformation C_1 of the aliphatic chain and by the backbone distance $\delta_6 = 2.1$ Å. The latter value shows that the backbone segment of LyR216 is stably H-bonded to the amide group of Gly220 in the crystallographic α-helical arrangement. Note in this context that LyR216 is located at the beginning of the C-terminal part of α-helix G just after the π-bulge at Ala215, which separates the two differently oriented parts of α-helix G.[40]

In the first three simulations, a conformational transition (marked by the dashed lines in Figure 4) occurred after 5, 25, and 15 ns, respectively. In these transitions, the initial conformation C_1 of the aliphatic chain in LyR216 changed into conformation C_2 or C_3. Correspondingly, in Figure 4, the distance $\delta_6(t)$ increases to 3.3 Å (C_2) or 3.8 Å (C_3), indicating that the associated H-bond is broken, i.e., that LyR216 has abandoned its original integration into α-helix G. The reverse transition back to C_1 was never observed. Thus, on a time scale of about 10 ns, the CHARMM22 model of BR predicts conformational transitions involving a partial unzipping of α-helix G.

A closer look at the first five distance trajectories $\delta_\alpha(t)$ in Figure 4 reveals that the CHARMM22 model of BR deviates from 1C3W in further structural details. These deviations show up on a much shorter time scale, i.e., during the initial relaxation into the conformation C_1. In C_1, the trajectories $\delta_4(t)$ and $\delta_5(t)$ are strictly anticorrelated, switching between values of 2.1 and 2.7 Å, respectively. These values show that the $RSBH^+$ is always H-bonded to one of the Asp85 oxygens. The trajectories indicate that the two oxygens exchange place about every 4 ns. Correspondingly, in C_1, the water molecules are found at much larger distances with W_3 remaining stably at 5.7 Å. W_1 and W_2 are seen to exchange every 1.2 ns their positions at distances of 2.8 and 4.3 Å from the Schiff base proton. In conformation C_2, the considered trajectories $\delta_\alpha(t)$ are similar except for a slightly larger distance (3.0 Å instead of 2.8 Å) of the closest water molecule. For C_3, however, the data in Figure 4 indicate a stable H-bond to either W_1 or W_2.

In summary, the CHARMM22 model of BR predicts either a decay of the stable H-bonded network displayed by Figure 2 (for C_1 and C_2) or a partial decay of the α-helix G (for C_3) or

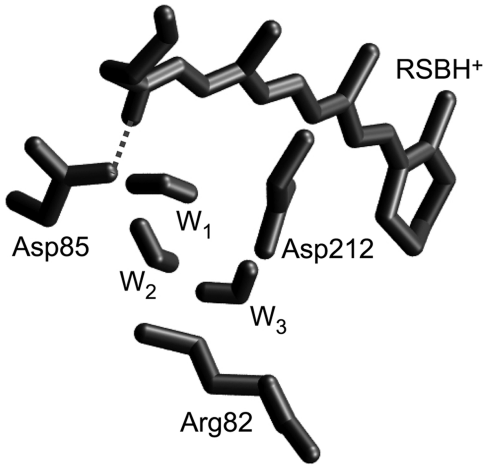

Figure 5. Typical structure of the chromophore binding pocket during those 50 ns of MD simulation with the CHARMM22 force field, during which the crystallographic conformation C_1 of LyR216 was maintained. The structure features an H-bond (gray dashed line) between Asp85 and the protonated Schiff base and is typical for the non-native conformation C_{nn} of the hydrogen bonded network.

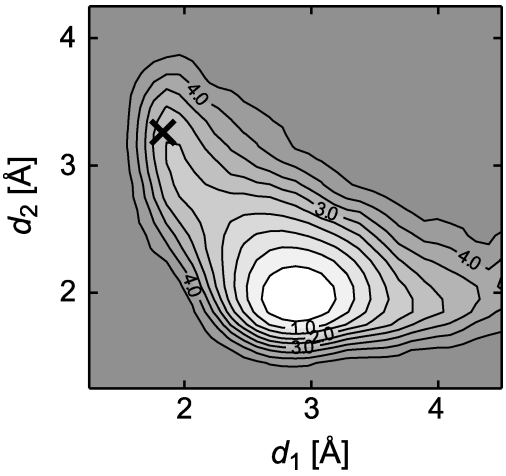

Figure 6. CHARMM22 free energy landscape $\Delta G(d_1,d_2)$ (in kcal/mol) for the conformation C_1 of the lysine chain obtained from 50 ns of MD simulation at 300 K. ΔG is a function of the distances between the Schiff base proton and the nearest oxygen of a water molecule (d_1) or of Asp85 (d_2). The black cross marks the values of these distances in the all-atom model 1C3W/MD of the crystallographic structure.[40]

both (for C_2). Figure 5 shows a typical snapshot from a CHARMM22 trajectory with LyR216 in the crystallographic conformation C_1. As expected above for a simulation with a nonpolarizable force field, the stable hydrogen bonded network displayed by Figure 2 has been replaced by a stable H-bond between the $RSBH^+$ and Asp85, characterizing the conformational state C_{nn}. Due to the strong association of the $RSBH^+$ with a single counterion and the well-known sensitivity of the $RSBH^+$ to counterion distance, such structures are invalid as starting points for DFT/MM calculations of the chromophore's IR spectra.[39]

The free energy landscape $\Delta G(d_1,d_2)$ depicted in Figure 6 provides a measure for the strength of the association between the $RSBH^+$ and Asp85 in the CHARMM22 simulations with lysine conformation C_1. $\Delta G(d_1,d_2)$ has been obtained from the first five trajectories $\delta_\alpha(t)$, whose smoothed versions are depicted in Figure 4, as described in Methods. According to Figure 6, $\Delta G(d_1,d_2)$ has a minimum at the H-bonding distance $d_2 \approx 2$ Å between Asp85 and the Schiff base proton which is characteristic for the non-native conformation C_{nn} of the hydrogen bonded

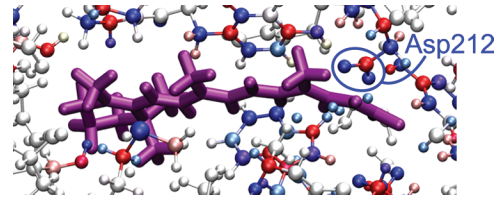

Figure 7. Polarization charges $Q_{pol} - Q_{CHARMM}$ in the chromophore binding pocket. Negative polarization charges are drawn in red, positive ones in blue (magenta: $RSBH^+$).

network. In contrast, the all-atom model 1C3W/MD (black cross in Figure 6) assigns a much larger value (3.3 Å) to d_2 and signifies the H-bond between the Schiff base and a water molecule by the small value $d_1 \approx 1.9$ Å. At the position of the cross, the free energy ΔG is about 3 kcal/mol above the minimum, indicating that the crystallographic structure represents only a rare fluctuation in MD simulations of 1C3W/MD with the CHARMM22 force field (note here once again that the crystallographic structure 1C3W/MD features the lysine conformation C_1 and a stable hydrogen bond between LyR216 and Gly220).

PBR Stability of 1C3W/MD. To check whether the use of a polarized force field, which should provide an improved description of the electrostatic potential within BR, can remove the CHARMM22 instability described above, we applied the iterative DFT/MM procedure outlined in Methods to the 23 residues making up the binding pocket of the BR chromophore. The root-mean-square deviation (rmsd) between the partial charges of the resulting PBR force field and the standard CHARMM22 charges was about a tenth of an elementary charge (0.13 e). Much larger (>0.2 e) than this 23 residue average were the local rmsd's for Asp85, Asp212, and Leu93. Still, sizable rmsd's were found at Met20, Met118, Tyr83, and Tyr57 (for detailed comparisons, see Tables 2−9 in the SI).

Figure 7 illustrates these results by highlighting the differences between the PBR and CHARMM22 partial charges. Considering specifically Asp212, one recognizes that additional negative charge is attracted by the positively charged chromophore and is shifted from the C_γ atom to the two terminal oxygen atoms. Thus, at Asp212, the PBR charge distribution differs from the CHARMM22 standard by an additional induced dipole pointing (as expected) away from the $RSBH^+$ for its improved solvatization. A similar geometry of induced dipoles is also observed at other residues.

Figure 8 shows the free energy landscape $\Delta G(d_1,d_2)$ obtained from a 50 ns simulation with the polarized force field PBR. Comparing this landscape visually with the CHARMM22 result in Figure 6, one immediately recognizes that the experimental H-bonded structure of the chromophore binding pocket (Figure 2) has been preserved in the PBR simulation. Now the minimum of $\Delta G(d_1,d_2)$ is found quite close to the experimental (low-temperature) structure indicated by the cross. Thus, the H-bond between the protonated Schiff base and a water molecule has apparently been quite stable during this extended MD simulation.

A look at Figure 9, which displays the trajectories $\delta_\alpha(t)$ of the six distances employed as measures for conformational stability (cf. Figure 4), immediately proves that the H-bonded network in the chromophore binding pocket remained rock-solid during the 50 ns of MD simulation with PBR. The only apparent dynamics is an occasional (every 6 ns) exchange of the water molecules W_1 and W_2 as hydrogen bonding partners of the $RSBH^+$. The distance δ_6 remains constantly small at 2.1 Å, proving that at LyR216 the α-helical structure of helix G was preserved and indicating that the lysine chain did not undergo

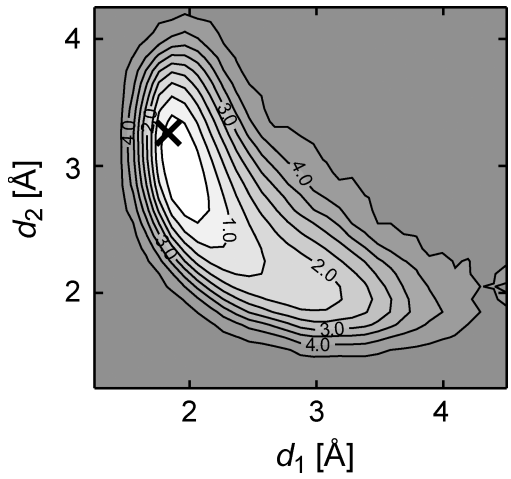

Figure 8. Free energy landscape $\Delta G(d_1,d_2)$ for the polarized force field PBR. For further explanation, see the text and the caption to Figure 6.

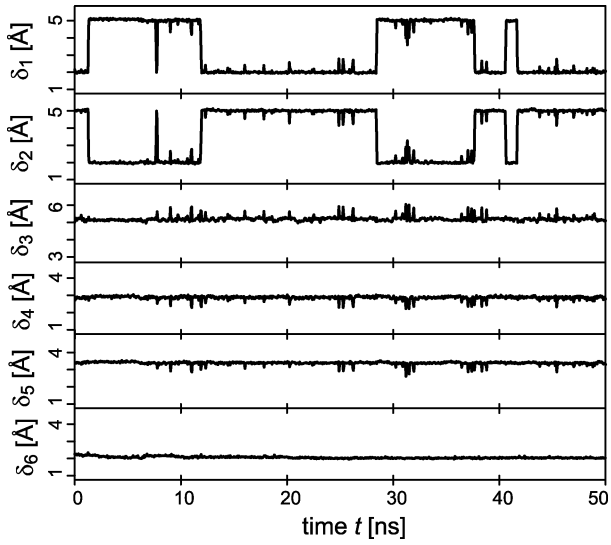

Figure 9. Trajectories of six distances $\delta_\alpha(t)$, from a 50 ns PBR-MD simulation at 300 K starting at the structure 1C3W/MD. For further explanations, see the caption to Figure 4.

any conformational transitions. In fact, a conformational classification of the torsional angles within the lysine chain has demonstrated that the initial conformation C_1 was maintained during the 50 ns of simulation (data not shown).

The above data have demonstrated that the electronic polarization of the $RSBH^+$ and of the surrounding residues can stabilize the chromophore binding pocket. For reasons discussed further above, we employed in the PBR simulation the standard nonpolarizable TIP3P model potential for the water molecules, thus neglecting possible polarization effects at these sites. To obtain an estimate on the size of these effects, we have applied our DFT/MM approach (after completion of the above MD study) also to the three water molecules in the binding pocket for the structure 1C3W/MD. Independently of the force field employed for the apoprotein (PBR or CHARMM22) and hardly varying with position and orientation (cf. Figure 2), we found that the dipole moments of these molecules were about 2.59 D instead of the 2.35 D characteristic for TIP3P. This value of 2.59 D is also larger than the average dipole moment of 2.41 D determined previously by the same DFT/MM approach for DFT water molecules in liquid MM water environments.[35]

This result came unexpected to us. In view of the strong local electric fields acting in bulk water on a given molecule, we had assumed that the mean field polarization coded into a bulk water model like TIP3P should suffice to describe also the polarization of a few molecules in a hydrophobic environment. However, within a nonpolar environment near the center of a membrane and within the rigid and tightly bound network characterizing the binding pocket, the local electric fields are apparently stronger than expected. Thus, for the water molecules, our PBR simulation has underestimated the energetic stability of the associated H-bond interactions by about 10%, implying that the H-bonded network of Figure 2 is even more stable than suggested by Figure 8. An improved estimate on the size of this additional stabilization would have required lengthy MD simulations with a correspondingly extended polarized force field covering water molecules with larger dipole moments. However, because the stabilization of the experimental BR structure through a polarized force field has already been demonstrated and because such simulations are associated with a considerable computational cost, we did not address this issue further.

Heterogeneity. The 50 ns PBR simulation did not show any signs of conformational instability (neither for the hydrogen bonded network nor for the lysine chain nor for helix G). Thus, the conformational transitions and the new conformational states observed in three of the four CHARMM22 simulations could have simply been an artifact of the CHARMM22 force field. On the other hand, one of the many DFT/MM geometry optimizations of the $RSBH^+$, which started at a snapshot from the PBR-MD trajectory and was carried out for the purpose of computing a vibrational spectrum [see part II of this work (DOI 10.1021/jp902432e)], had accidentally also shown a transition of the lysine chain into a different conformation. Therefore, we were not sure as to whether other conformational states of the lysine chain are accessible at room temperature in BR.

However, if other conformational substates should actually exist in the 300 K equilibrium ensemble, then we had to expect from our 50 ns PBR simulation that they are separated by substantial free energy barriers from the crystallographic conformation. Because of the height of these barriers, a straightforward extension of simulation times offered no chance for a valid estimate of their possible contribution and alternative sampling techniques were required. Conventional replica exchange techniques[86,87] are computationally very costly and cannot guarantee the convergence of the sampling within the necessarily limited simulation times (see, e.g., ref 91 for a discussion). Therefore, we designed a Hamiltonian replica exchange (HRE) technique that concentrates on the few degrees of freedom within the lysine chain and therefore opens the chance that the 300 K equilibrium ensemble of lysine configurations can be sampled (see Methods).

The 30 ns of HRE sampling yielded a 300 K ensemble of lysine configurations, whose structure was analyzed by the hierarchical clustering procedures described in Methods. The SI presents details of the corresponding results for various levels of resolution. Here, we restrict our attention to a coarse level of resolution, at which the generalized HRE ensemble of lysine configurations is characterized by three main conformational states C_i, $i \in \{1, 2, 3\}$. These states are characterized by certain combinations $\Psi_i \in [0, 2\pi]^5$ of the five torsional angles within the lysine chain. For the recovery of the corresponding complete structures, the 300 K trajectories $\Psi(t)$ were scanned for most similar points $\Psi(t_i)$ and the snapshots at these time points t_i were chosen as prototypical structures. Figure 10 shows for each of the three main conformations the thus obtained prototypical

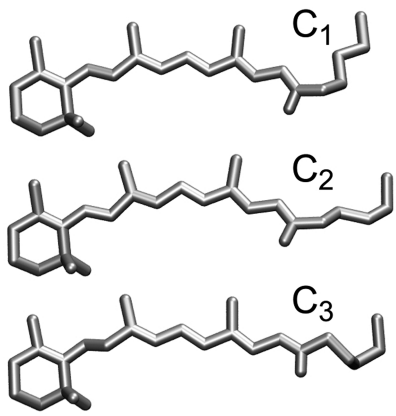

Figure 10. The three conformations of LyR216 dominating the PBR equilibrium ensemble at 300 K as determined by a hierarchical cluster analysis. C_1 is the conformation found in the X-ray structure 1C3W, and conformations C_2 and C_3 are alternate conformations previously observed in the 300 K simulation with the CHARMM22 force field (cf. Figure 4). The drawings cover the heavy atoms (and the Schiff base proton) within the LyR216 side chain.

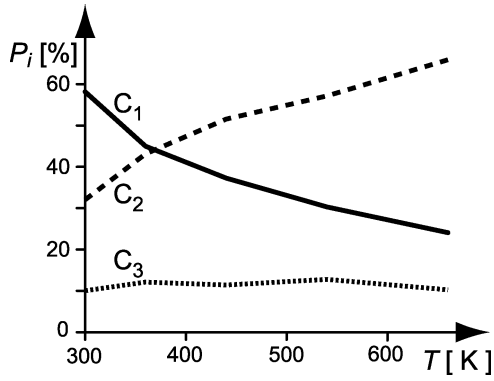

Figure 11. Occupancies P_i of the three conformational states C_i determined in generalized ensemble at the five replica temperatures $T \in \{300, 360, 440, 540, 660\ \mathrm{K}\}$ during the last 25 ns of HRE sampling.

structures of residue LyR216 (note that we have used this three-state classifier repeatedly in the previous sections).

In the generalized HRE ensemble, the conformational states C_i occur at different relative frequencies P_i, which depend on the temperature T of the respective replica. Although in the HRE setting only the replica at the target temperature $T_0 = 300$ K is of key physical importance, it is nevertheless instructive to consider the temperature dependence of the state occupancies $P_i(T)$. Figure 11 shows the corresponding data, which were derived from the last 25 ns of HRE sampling. The first 5 ns were considered as a relaxation phase because all replicas had been initialized at the model 1C3W/MD belonging to conformation C_1. At T_0, state C_1 is dominant (58%), C_2 represents a considerable population P_i (32%), and C_3 a minor (10%) population P_i. Interestingly, the populations P_i of the two frequent conformations C_1 and C_2 show an opposite temperature dependence: P_1 decreases whereas P_2 increases with T. Thus, it seems that C_1 is enthalpically and C_2 entropically favored.

This interpretation agrees with further observations. (i) The hierarchical classification tree depicted in Figure 15 of the SI shows a strong splitting of the class C_2 into many substates at finer resolutions. In contrast, the class C_1 does not show a similarly strong splitting. (ii) The average extension of the lysine chain differs in the various states. From the PBR ensemble at 300 K, we extracted for the distance δ_7 between the Schiff base nitrogen and the C_α atom of LyR216 the values 5.6 Å (C_1), 5.4 Å (C_2), and 4.7 Å (C_3). Applying the concepts of entropic springs, the most extended (crystallographic) conformation C_1 is likely to be compatible with fewer configurations of the aliphatic chain than the shorter conformation C_2 and, therefore, should represent a lower entropy state. Note that at very short distances δ_7 the number of thermally accessible configurations is expected to decrease once again, as seems to be the case for C_3. (iii) The shorter length δ_7 of the lysine chain in conformations C_2 and C_3 is always associated with an elongated distance δ_6, indicating a broken α-helical H-bond between LyR216 and Gly220 (HRE data for δ_6 not shown, but see Figure 4 and the SI). Thus, the intact H-bond in C_1 should enthalpically favor this state.

Discussion

For BR, the HRE results predict that the (crystallographic) state C_1 is, in fact, dominantly populated at the low temperatures (100 K) of the X-ray data collection and that other conformations will become increasingly important at physiological temperatures. To check this issue, we have applied our classifier to the 12 room-temperature NMR structures, which are considered as the best refinement results for the all-*trans* $RSBH^+$.[48] We found that three of these NMR structures are classified as C_1 and the remaining nine structures as C_2. In view of the fact that the NMR refinement employs an MD-based simulated annealing procedure, the dominance of the entropically favored high-temperature conformation C_2 in the NMR ensemble is no surprise (for further details, see the SI). However, independent of this detail, the ensemble of refined NMR structures has thus shown that the NMR data are compatible with the lysine conformations C_1 and C_2. Therefore, these data are also compatible with the results of our HRE simulations.

From the conformational analysis of the NMR results, one then expects that the NMR structures should show the broken α-helical H-bond at LyR216, which the MD simulations consistently predict as a correlate of conformation C_2. Unfortunately the NMR structures cannot furnish such a result, because the H-bond distances within the helices had been restrained to the crystallographic values in the final phase of NMR refinement.[48] Thus, the NMR structures cannot answer the important question as to what extent the C_2 conformation of the lysine chain is correlated with a melting of helix G near LyR216. Note in this connection that this local melting would be impeded, if helix G were α-helically intact. However, because of the π-bulge at Ala215, helix G is kinked with LyR216 marking the start of a new α-helical segment. It is well-known that melting disorder preferentially occurs at the ends of such segments. Physiologically, the π-bulge apparently creates an enhanced conformational flexibility for the covalent linkage between the chromophore and the $RSBH^+$.

In summary, the HRE results have clearly shown that the two additional conformations of the lysine chain encountered in the CHARMM22 simulations are also elements of the 300 K ensemble belonging to the PBR force field. Furthermore, they have demonstrated that the populations of these conformational states are temperature dependent. Here, particularly the crystallographic conformation C_1 is favored at low temperatures and the alternative conformation C_2, which dominates the NMR ensemble, is increasingly populated at higher (i.e., physiological) temperatures. Note at this point that the Schiff base stays stably hydrogen bonded to a water molecule in all alternative conformations as long as one employs the polarized force field PBR.

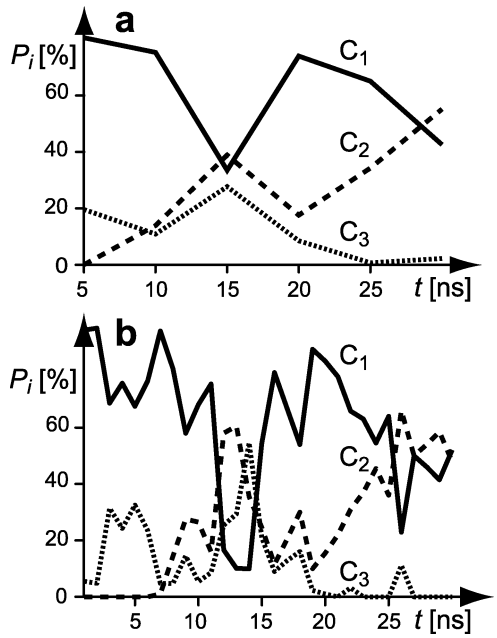

Figure 12. Temporal changes of the time-average occupancies $\langle P_i \rangle_{\Delta t}(t_k)$ of the three conformational states C_i in the 300 K replica during the 30 ns of HRE. The occupancies are given at times $t = k\Delta t$, $k = 1, 2, ...$, with the averaging times (a) $\Delta t = 5$ ns and (b) $\Delta t = 1$ ns.

Two important questions remain. One pertains to the mean first passage times of transitions between the conformations and the other to the accuracy of our estimates on the populations P_i at physiological temperatures. Unfortunately, we cannot provide quantitative and statistically sound answers to these questions, because the associated computational cost is intractable for our means.

Concerning the transitions between the conformational states of the lysine chain, we solely can state that we have never observed any such transition within our 300 K PBR-MD simulations. Neither the 50 ns simulation of conformation C_1 (cf. Figure 9) nor two further 20 ns simulations, which were initialized at conformations C_2 and C_3, respectively, showed any sign of a conformational transition into a different state (the latter simulations are documented in the SI). Thus, the lifetimes of the lysine conformations C_i must be larger than about 0.1 μs. However, these lifetimes may well be several orders of magnitude larger than that (e.g., several μs).

Concerning the question as to what extent the 30 ns HRE sampling has converged toward the equilibrium state of the generalized ensemble, one cannot give a definite answer. The reason for this uncertainty is rather subtle: If the conformational transitions were exclusively confined to the lysine chain (which was our working hypothesis), the huge number of transitions observed during the HRE sampling within that chain would guarantee convergence. However, as we have detected during our analysis of the HRE trajectories (see above), the transition from C_1 to alternative conformations is always associated with a breaking of an H-bond in helix G. However, this helix was excluded from the rapid HRE sampling by our initial partitioning of the system into "hot" and "cool" regions and its conformational dynamics proceeds at the slow speed of a 300 K ensemble. Therefore, despite our extended sampling, the convergence cannot be guaranteed and valid error bounds for the populations $P_i(T_0)$ cannot be given.

As an illustration for the difficulties of achieving convergence, consider Figure 12. At the coarse time resolution of 5 ns (Figure 12), it may seem as if state C_1 tends to become less populated with increasing HRE simulation time than state C_2. Furthermore, state C_3 even seems to disappear. However, at the finer time resolution of 1 ns, the large sizes of the occupancy fluctuations become apparent, indicating that such conclusions are premature.

Concerning the sizes of the populations at 300 K, the HRE results thus solely prove that there are two similarly frequent conformations C_1 and C_2, whereas other conformations occur at a much smaller frequency. Interestingly, the opposite behavior of the temperature dependences of C_1 and C_2 documented in Figure 11 is a much more stable result of the HRE simulations. Similar curves were obtained already when we had only a total of 20 ns simulation time for statistical analysis.

The conformational heterogeneity thus identified for the light-adapted state BR_{568} has important implications for the photocycle. Different initial conformations of the lysine chain will quite certainly lead to conformationally different photoproducts, because the photoisomerization involving the C_{13}=C_{14} bond is mechanically coupled to lysine chain motions. In line with these concepts and the above results, a conformational heterogeneity has been postulated already two decades ago by Diller and Stockburger[92] from room-temperature time-resolved resonance Raman spectroscopy. These authors interpreted their spectra of the L_{550} intermediate, which shows up a few μs after photoisomerization, in terms of two different conformational states for BR_{568} and L_{550} (called α and β). As relative occupancies, they estimated 58 and 42%, respectively. As key differences, they identified the kinetics of appearance and decay of the L intermediate for the two conformations (L_α being fast and L_β slow).[93] Because of the statistical uncertainties in our calculation of relative populations (see above), we unfortunately cannot be sure, which of our conformations C_1 and C_2 belongs to α and which to β.

In agreement with the concept of a conformational heterogeneity persisting up to the L state, a recent analysis of the BR photocycle kinetics has led Zimanyi et al.[94] to the conclusion that "no photocycle scheme with a single L intermediate is acceptable". However, we do not share the strong conviction of Diller and Stockburger[92] that the conformational heterogeneity must persist also to the millisecond time scale of the photocycle (this view has been most recently reiterated by Hendler et al.[95] on the basis of yet another analysis of the photocycle kinetics). If the conformational transitions within the lysine chain should proceed, e.g., on the 100 μs time scale, then two initially different (and at L still present) cycles could subsequently merge. However, independent of this detail, one should remark that during the past decades the BR community has been quite reluctant to accept the additional complication of a conformational heterogeneity for BR (see the review by Lanyi[3] for a discussion). However, the results of the HRE simulations forced us to give up our corresponding resistance.

As is the case in any MD approach, the predictive power of our study remains limited by force field uncertainties and by the sampling problem. To gain an improved predictive power, we have done our best to partially master these problems specifically for the given case of BR.

Addressing the force field problem, we have calculated by DFT/MM the polarized force field PBR for the reference structure 1C3W/MD. Now one could suspect that this force field preferentially stabilizes BR in the crystallographic conformation C_1. To check this issue, we have additionally calculated another polarized force field PBR(C_2) for a reference structure representative for conformation C_2. This structure was obtained as a snapshot from a PBR trajectory initialized and staying in C_2. As shown in the SI, with PBR(C_2), the 300 K free energy

landscape $\Delta G(d_1,d_2)$ of conformation C_2 is nearly identical to that obtained with PBR.

Addressing the sampling problem, we have designed a HRE procedure for the lysine conformations. This procedure actually solved a part of the problem, because it proved the existence and important properties of alternative conformations. However, it also fell short of solving it completely because we had chosen the region of "hot" sampling a little too small.

Summary and Outlook

Driven by our desire to construct a MD simulation system, which allows us to sample the room-temperature fluctuations within the chromophore binding pocket of BR in a reliable fashion, we have (i) derived the structure-adapted polarized force field PBR from self-consistent "moving domain" DFT/MM computations of partial charge distributions and have (ii) designed and applied a Hamiltonian replica exchange approach for probing the equilibrium fluctuations of the lysine chain, which is the covalent linkage between the $RSBH^+$ and the protein backbone.

For physiological temperatures, our HRE approach has revealed the coexistence of at least two major conformations C_1 and C_2, whose contributions to the conformational ensemble show a distinct and opposite temperature dependence. Here, the enthalpically favored (crystallographic[40]) conformation C_1 dominates at low temperatures, whereas the entropically favored conformation C_2 (featuring a more flexible lysine chain) dominates at elevated temperatures and in the NMR ensemble.[48] The enhanced flexibility of C_2 is due to a local melting of helix G at LyR216, which is enabled by a preformed kink ("π-bulge") within that helix at Ala215.

According to the room-temperature PBR-MD simulations, the conformations C_1 and C_2 both preserve the stable H-bonded network generated by the small water cluster within the chromophore binding pocket. Surprisingly, a DFT/MM treatment has demonstrated that the dipole moments of the H_2O molecules within that cluster are larger than in a bulk liquid, thus indicating stiffer binding interactions. The PBR-MD simulations have also shown that at room temperature transitions between C_1 and C_2 occur on time scales above 0.1 μs. The thus emerging conformational heterogeneity of BR supports previous (and persistently doubted) interpretations of time-resolved resonance Raman spectra.[92]

The success of generating a reasonably stable MD model of BR now has paved the way toward the DFT/MM computation of the BR vibrational spectra, which will be tackled in part II of this work (DOI 10.1021/jp902432e). Why this task is still a highly interesting challenge will be discussed in the introductory remarks to part II (DOI 10.1021/jp902432e).

Acknowledgment. The authors gratefully acknowledge financial support by the Deutsche Forschungsgemeinschaft (SFB 533, projects C1 and C3) and valuable discussions with B. Schropp concerning the properties of water.

Supporting Information Available: On 14 pages, the SI provides 8 tables, 10 figures, and text explaining and discussing the additional material. In the above text, the contents of the SI have been addressed at various locations. The SI specifies the force field PBR (tables 2−9), explains the classification of the lysine conformations (including the quoted NMR data, pp S5−S8), and presents and discusses results of MD simulations for the three conformations C1−C3 and for different force fields (pp. S9−S13). This material is available free of charge via the Internet at http://pubs.acs.org.

References and Notes

(1) Oesterhelt, D.; Stoeckenius, W. *Nat. New Biol.* **1971**, *233*, 149–152.
(2) Oesterhelt, D.; Stoeckenius, W. *Proc. Natl. Acad. Sci. U.S.A.* **1973**, *70*, 2853–2857.
(3) Lanyi, J. K. *Annu. Rev. Physiol.* **2004**, *66*, 665–688.
(4) Haupts, U.; Tittor, J.; Oesterhelt, D. *Annu. Rev. Biophys. Biomol. Struct.* **1999**, *28*, 367–399.
(5) Garczarek, F.; Gerwert, K. *Nature* **2006**, *439*, 109–112.
(6) McCamant, D.; Kukura, P.; Mathies, R. *J. Phys. Chem. B* **2005**, *105*, 10449–10457.
(7) Herbst, J.; Heyne, K.; Diller, R. *Science* **2002**, *297*, 822–825.
(8) Siebert, F.; Hildebrandt, P. *Vibrational spectroscopy in life science*; Wiley-VCH: Weinheim, Germany, 2007.
(9) Smith, S. O.; Myers, A.; Pardoen, J.; Winkel, C.; Mulder, P.; Lugtenburg, J.; Mathies, R. *Proc. Natl. Acad. Sci. U.S.A.* **1984**, *81*, 2055–2059.
(10) Alshuth, T.; Stockburger, M. *Photochem. Photobiol.* **1986**, *43*, 55–66.
(11) Fodor, S. P. A.; Pollard, W. T.; Gebhard, R.; van den Berg, E. M. M.; Lugtenburg, J.; Mathies, R. A. *Proc. Natl. Acad. Sci. U.S.A.* **1988**, *85*, 2156–2160.
(12) Siebert, F. *Methods Enzymol.* **1995**, *246*, 501–526.
(13) Engelhard, M.; Gerwert, K.; Hess, B.; Kreutz, W.; Siebert, F. *Biochemistry* **1985**, *24*, 400–407.
(14) Zscherp, C.; Heberle, J. *J. Phys. Chem. B* **1997**, *101*, 10542–10547.
(15) Curry, B.; Broek, A.; Lugtenburg, J.; Mathies, R. A. *J. Am. Chem. Soc.* **1982**, *104*, 5274–5286.
(16) Smith, S. O.; Myers, A.; Mathies, R.; Pardoen, J.; Winkel, C.; van den Berg, E.; Lugtenburg, J. *Biophys. J.* **1985**, *47*, 653–664.
(17) Groβjean, M. F.; Tavan, P.; Schulten, K. *Eur. Biophys. J.* **1989**, *16*, 341–349.
(18) Fahmy, K.; Groβjean, M. F.; Siebert, F.; Tavan, P. *J. Mol. Struct.* **1989**, *214*, 257–288.
(19) Groβjean, M. F.; Tavan, P.; Schulten, K. *J. Phys. Chem.* **1990**, *94*, 8059–8069.
(20) Groβjean, M. F.; Tavan, P. *J. Chem. Phys.* **1988**, *88*, 4884–4896.
(21) Hohenberg, P.; Kohn, W. *Phys. Rev.* **1964**, *136*, B864−B870.
(22) Kohn, W.; Sham, L. J. *Phys. Rev.* **1965**, *140*, A1133−A1138.
(23) Frisch, M. J.; et al. *Gaussian 92*, revision F.2; Gaussian, Inc.: Pittsburgh PA, 1993.
(24) Nonella, M.; Tavan, P. *Chem. Phys.* **1995**, *199*, 19–32.
(25) Zhou, X.; Mole, S. J.; Liu, R. *Vib. Spectrosc.* **1996**, *12*, 73–79.
(26) Neugebauer, J.; Hess, B. *J. Chem. Phys.* **2004**, *118*, 7215–7225.
(27) Schmitz, M.; Tavan, P. On the art of computing the IR spectra of molecules in condensed phase. In *Modern methods for theoretical physical chemistry of biopolymers*; Starikov, E. B., Tanaka, S., Lewis, J., Eds.; Elsevier: Amsterdam, The Netherlands, 2006.
(28) Eichinger, M.; Tavan, P.; Hutter, J.; Parrinello, M. *J. Chem. Phys.* **1999**, *110*, 10452–10467.
(29) Nonella, M.; Mathias, G.; Eichinger, M.; Tavan, P. *J. Phys. Chem. B* **2003**, *107*, 316–322.
(30) Nonella, M.; Mathias, G.; Tavan, P. *J. Phys. Chem. A* **2003**, *107*, 8638–8647.
(31) Klähn, M.; Mathias, G.; Koetting, C.; Nonella, M.; Schlitter, J.; Gerwert, K.; Tavan, P. *J. Phys. Chem. A* **2004**, *108*, 6186–6194.
(32) Schmitz, M.; Tavan, P. *J. Chem. Phys.* **2004**, *121*, 12233–12246.
(33) Schmitz, M.; Tavan, P. *J. Chem. Phys.* **2004**, *121*, 12247–12258.
(34) Schrader, T. E.; Schreier, W. J.; Cordes, T.; Koller, F. O.; Babitzki, G.; Denschlag, R.; Renner, C.; Dong, S.; Löweneck, M.; Moroder, L.; Tavan, P.; Zinth, W. *Proc. Natl. Acad. Sci. U.S.A.* **2007**, *104*, 15729–15734.
(35) Schropp, B.; Tavan, P. *J. Phys. Chem. B* **2008**, *112*, 6233–6240.
(36) Schultheis, V.; Reichold, R.; Schropp, B.; Tavan, P. *J. Phys. Chem. B*, submitted for publication, 2008.
(37) Warshel, A.; Levitt, M. *J. Mol. Biol.* **1976**, *103*, 227–249.
(38) Klähn, M.; Schlitter, J.; Gerwert, K. *Biophys. J.* **2005**, *88*, 3829–3844.
(39) Eichinger, M. Berechnung molekularer Eigenschaften in komplexer Lösungsmittelumgebung: Dichtefunktionaltheorie kombiniert mit einem Molekularmechanik-Kraftfeld. Doktorarbeit, Ludwig-Maximilians Universität München, Germany, 1999.
(40) Luecke, H.; Schobert, B.; Richter, H.-T.; Cartailler, J.-P.; Lanyi, J. K. *J. Mol. Biol.* **1999**, *291*, 899–911.
(41) Grigorieff, N.; Ceska, T. A.; Downing, K. H.; Baldwin, J. M.; Henderson, R. *J. Mol. Biol.* **1996**, *259*, 393–421.
(42) Essen, L.-O.; Siegert, R.; Lehmann, W. D.; Oesterhelt, D. *Proc. Natl. Acad. Sci. U.S.A.* **1998**, *95*, 11673–11678.
(43) Hildebrandt, P.; Stockburger, M. *Biochemistry* **1984**, *23*, 5539–5548.
(44) de Groot, H. J. M.; Harbison, S.; Herzfeld, J.; Griffin, R. G. *Biochemistry* **1989**, *28*, 3346–3353.
(45) MacKerell, A.; et al. *J. Phys. Chem. B* **1998**, *102*, 3586–3616.

(46) Alshuth, T. Kinetische und strukturelle Untersuchungen am Chromophor von Bacteriorhodopsin mit Hilfe zeitaufgelöster Resonanz-Raman-Spektroskopie. Doktorarbeit, Goerg-August Universität, Göttingen, 1985.

(47) Gerwert, K. Transduktion der Lichtenergie in Protonen-Transfer-Reaktionen beim Bacteriorhodopsin: Eine Untersuchung mit Hilfe der zeitaufgelösten IR- und statischen FTIR-Differenzspektroskopie. Doktorarbeit, Albert-Ludwigs-Universität Freiburg im Breisgau, 1985.

(48) Patzelt, H.; Simon, B.; terLaak, A.; Kessler, B.; Kühne, R.; Schmieder, P.; Oesterhelt, D.; Oschkinat, H. *Proc. Natl. Acad. Sci. U.S.A.* **2002**, *99*, 9765–9770.

(49) Baudry, J.; Tajkhorshid, E.; Molnar, F.; Phillips, J.; Schulten, K. *J. Phys. Chem. B* **2001**, *105*, 905–918.

(50) Kandt, C.; Schlitter, J.; Gerwert, K. *Biophys. J.* **2004**, *86*, 705–717.

(51) Grudinin, S.; Büldt, G.; Gordeliy, V.; Baumgaertner, A. *Biophys. J.* **2005**, *88*, 3252–3261.

(52) Berendsen, H. J. C.; van der Spoel, D.; van Drunen, R. *Comput. Phys. Commun.* **1995**, *91*, 43–56.

(53) Lindahl, E.; Hess, B.; van der Spoel, D. *J. Mol. Model.* **2001**, *7*, 306–317.

(54) Jorgensen, W. L.; Chandrasekhar, J.; Madura, J. D.; Impey, R. W.; Klein, M. L. *J. Chem. Phys.* **1983**, *79*, 926–935.

(55) Hayashi, S.; Tajkhorshid, E.; Schulten, K. *Biophys. J.* **2002**, *83*, 1281–1297.

(56) Rick, S. W.; Stuart, S. J.; Berne, B. J. *J. Chem. Phys.* **1994**, *101*, 453–462.

(57) Hayashi, S.; Ohmine, I. *J. Phys. Chem. B* **2000**, *104*, 10678–10691.

(58) Tavan, P.; Carstens, H.; Mathias, G. Molecular dynamics simulations of proteins and peptides: Problems, achievements, and perspectives. In *Protein Folding Handbook. Part 1*; Buchner, J., Kiefhaber, T., Eds.; Wiley-VCH: Weinheim, Germany, 2005.

(59) Warshel, A.; Kato, M.; Pisliakov, A. V. *J. Chem. Theory Comput.* **2007**, *3*, 2034–2045.

(60) Brünger, A. "X-PLOR Manual", The Howard Hughes Medical Institute and Department of Molecular Biophysics and Biochemistry, Yale University, New Haven, CT, 1992.

(61) Braiman, M.; Mogi, T.; Marti, T.; Stern, L.; Khorana, H.; Rothschild, K. *Biochemistry* **1988**, *27*, 8516–8520.

(62) Gerwert, K.; Hess, B.; Soppa, J.; Oesterhelt, D. *Proc. Natl. Acad. Sci. U.S.A.* **1989**, *86*, 4943–4947.

(63) Metz, G.; Siebert, F.; Engelhard, M. *FEBS Lett.* **1992**, *303*, 237–241.

(64) Spassov, V. Z.; Luecke, H.; Bashford, D.; Gerwert, K. *J. Mol. Biol.* **2001**, *312*, 203–219.

(65) Roux, B.; Nina, M.; Pomes, R.; Smith, J. C. *Biophys. J.* **1996**, *71*, 670–681.

(66) Tavan, P.; Schulten, K.; Oesterhelt, D. *Biophys. J.* **1985**, *47*, 415–430.

(67) Tajkhorshid, E.; Paizs, B.; Suhai, S. *J. Phys. Chem. B* **1999**, *103*, 4518–4527.

(68) Tajkhorshid, E.; Baudry, J.; Schulten, K.; Suhai, S. *Biophys. J.* **2000**, *78*, 683–693.

(69) Mathias, G.; Egwolf, B.; Nonella, M.; Tavan, P. *J. Chem. Phys.* **2003**, *118*, 10847–10860.

(70) Niedermeier, C.; Tavan, P. *J. Chem. Phys.* **1994**, *101*, 734–748.

(71) Niedermeier, C.; Tavan, P. *Mol. Simul.* **1996**, *17*, 57–66.

(72) Eichinger, M.; Grubmüller, H.; Heller, H.; Tavan, P. *J. Comput. Chem.* **1997**, *18*, 1729–1749.

(73) Grubmüller, H.; Tavan, P. *J. Comput. Chem.* **1998**, *19*, 1534–1552.

(74) Kräutler, V.; van Gunsteren, W. F.; Hünenberger, P. *J. Comput. Chem.* **2001**, *22*, 501–508.

(75) Berendsen, H. J. C.; Postma, J. P. M.; van Gunsteren, W. F.; DiNola, A.; Haak, J. R. *J. Chem. Phys.* **1984**, *81*, 3684–3690.

(76) Lingenheil, M.; Denschlag, R.; Reichold, R.; Tavan, P. *J. Chem. Theory Comput.* **2008**, *4*, 1293–1306.

(77) Gascon, J. A.; Leung, S. S. F.; Batista, E. R.; Batista, V. S. *J. Chem. Theory Comput.* **2006**, *2*, 175–186.

(78) Hutter, J.; Alavi, A.; Deutsch, T.; Bernasconi, M.; Goedecker, S.; Marx, D.; Tuckerman, M.; Parinello, M. "CPMD V3.9", Copyright IBM Corp and MPI für Festkörperforschung Stuttgart, 2004; www.cpmd.org.

(79) Becke, A. D. *Phys. Rev. A* **1988**, *38*, 3098–3100.

(80) Perdew, J.; Yue, W. *Phys. Rev. B* **1986**, *33*, 8800–8802.

(81) Troullier, N.; Martins, J. L. *Phys. Rev. B* **1991**, *43*, 1993–2005.

(82) Singh, U. C.; Kollman, P. A. *J. Comput. Chem.* **1984**, *5*, 129–145.

(83) Sugita, Y.; Kitao, A.; Okamoto, Y. *J. Chem. Phys.* **2000**, *113*, 6042–6051.

(84) Fukunishi, H.; Watanabe, O.; Takada, S. *J. Chem. Phys.* **2002**, *116*, 9058–9067.

(85) Liu, P.; Kim, B.; Friesner, R. A.; Berne, B. J. *Proc. Natl. Acad. Sci. U.S.A.* **2005**, *102*, 13749–13754.

(86) Hansmann, U. H. E. *Chem. Phys. Lett.* **1997**, *281*, 140.

(87) Sugita, Y.; Okamoto, Y. *Chem. Phys. Lett.* **1999**, *314*, 141–151.

(88) Carstens, H.; Renner, C.; Milbradt, A. G.; Moroder, L.; Tavan, P. *Biochemistry* **2005**, *44*, 4829–4840.

(89) Kloppenburg, M.; Tavan, P. *Phys. Rev. E* **1997**, *55*, 2089–2092.

(90) Albrecht, S.; Busch, J.; Kloppenburg, M.; Metze, F.; Tavan, P. *Neural Networks* **2000**, *13*, 1075–1093.

(91) Denschlag, R.; Lingenheil, M.; Tavan, P. *Chem. Phys. Lett.* **2008**, *458*, 244–248.

(92) Diller, R.; Stockburger, M. *Biochemistry* **1988**, *27*, 7641–7651.

(93) Certain details of the conclusions of Diller and Stockburger[92] were subsequently revised in a time-resolved Resonance-Raman study[96] on the pH dependence of the BR photocycle intermediates following L without, however, affecting the main result on the heterogeneity of L.

(94) Zimanyi, L.; Saltiel, J.; Brown, L. S.; Lanyi, J. K. *J. Phys. Chem. A* **2006**, *110*, 2318–2321.

(95) Hendler, R. W.; Shrager, R. I.; Meuse, C. W. *Biochemistry* **2008**, *47*, 5406–5416.

(96) Eisfeld, W.; Pusch, C.; Diller, R.; Lahrmann, R.; Stockburger, M. *Biochemistry* **1993**, *32*, 7196–7215.

JP902428X